

Missing links prediction: comparing machine learning with physics-rooted approaches

Francesca Santucci,^{1,*} Giulio Cimini,^{2,3} and Tiziano Squartini^{1,4,5}

¹*IMT School for Advanced Studies, P.zza San Francesco 19, 55100 Lucca (Italy)*

²*'Enrico Fermi' Research Center (CREF), Via Panisperna 89A, 00184 Rome (Italy)*

³*Department of Physics and INFN, 'Tor Vergata' University of Rome, 00133 Rome (Italy)*

⁴*Scuola Normale Superiore, P.zza dei Cavalieri 7, 56126 Pisa (Italy)*

⁵*INdAM-GNAMPA Istituto Nazionale di Alta Matematica 'Francesco Severi', P.le Aldo Moro 5, 00185 Rome (Italy)*

(Dated: February 2, 2026)

An active research line within the broader field of network science is the one concerning link prediction. Close in scope to network reconstruction, link prediction targets specific connections with the aim of uncovering the missing ones, as well as predicting those most likely to emerge in the future, from the available information. In this paper, we consider two families of methods, i.e. those rooted in statistical physics and those based upon machine learning: the members of the first family identify missing links as the most probable non-observed ones, the probability coefficients being determined by solving maximum-entropy benchmarks over the accessible network structure; the members of the second family, instead, associate the presence of single edges to explanatory node-specific variables. Running likelihood-based models such as the Configuration Model, or one of its many fitness-based variants, in parallel with the Gradient Boosting Decision Tree algorithm reveals that the former's accuracy is comparable to (and sometimes slightly higher than) the latter's. Such a result confirms that white-box algorithms are viable competitors to the currently available black-box ones, being computationally faster and more interpretable than the latter.

PACS numbers: 89.75.Fb; 02.50.Tt

I. INTRODUCTION

Link prediction is an active research line within the broader field of network science. Close in scope to network reconstruction [1], link prediction targets specific connections, aiming to uncover missing ones and predict those most likely to emerge in the future [2]. Generally speaking, the link prediction problem can be stated by asking the following question: *given a supposedly incomplete snapshot of a network, can the most-likely 'yet-to-come' edges be predicted?* Such an issue is relevant in many research areas, such as those concerning socio-economic and financial networks [3–7]: knowing the structure of the commercial partnerships between firms or of the financial exchanges between banks is, in fact, relevant for a number of reasons, such as quantifying the risk associated with the propagation of a shock [7–9].

Link prediction algorithms rank unconnected node pairs on the basis of a *score*: while some methods rely on purely structural information, others admit external information such as node- and edge-specific features.

The simplest framework to carry out link prediction includes the so-called *similarity-based* algorithms: scores, here, are induced by some measure of similarity between nodes; to this aim, *local* [3, 10, 11], *quasi-local* [11] or *global* [12–15] information - such as the degree, the degree of common neighbours or the length of paths connecting any two nodes - has been employed [2, 3, 11, 16].

A more refined framework includes the so-called

likelihood-based algorithms, defined by a likelihood function whose maximisation provides the probability that any two nodes are connected; this is usually achieved by assuming that a certain amount of information is accessible, hence treating it as a constraint to account for: examples are provided by the methods relying on a graph modular structure [17, 18] or those induced by entropy maximisation [6, 19].

More computer science-oriented approaches are, instead, defined by models whose parameters represent node- and edge-specific features [2, 20, 21]: specifying a model, thus, amounts to learning a function that determines the probability for nodes i and j to be connected while taking as inputs the two vectors \mathbf{f}_i and \mathbf{f}_j of node-specific features (e.g. the sales, the number of employees, the degree of firm i and firm j) and the vector \mathbf{g}_{ij} of edge-specific features (e.g. the geographic distance of the two firms, the volume of sector-specific exchanges).

In all cases, algorithms are trained on a portion of the whole network, i.e. the *training set*, while the prediction is carried out on the links of the unobserved part, i.e. the *test set*.

The present work is devoted to comparing the performance of different link prediction methods in recovering the missing portion of the edge set of the (binary, undirected representation of the) World Trade Web and of the electronic Market for Interbank Deposits. The framework is the same as in [6], where the training set coincides with the whole network apart from a percentage of deleted connections and the proper prediction exercise

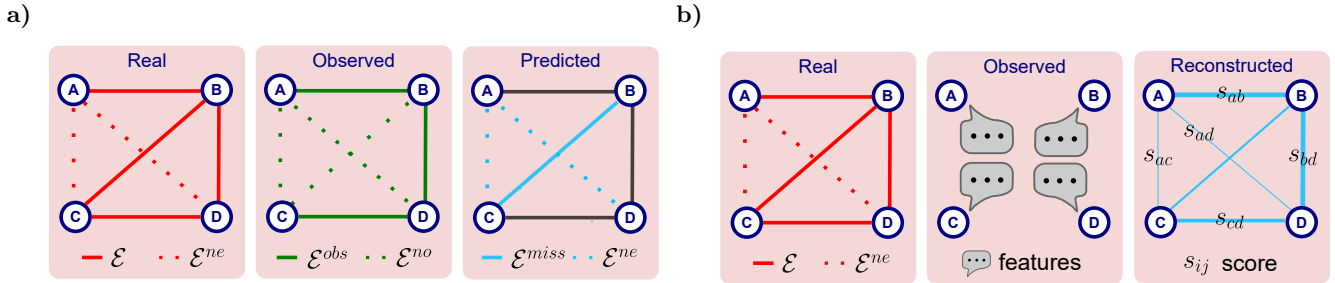


Figure 1: Visual representation of the framework adopted to carry out link prediction in [6]. Panel **a**: the red, solid lines indicate the empirical edges while the red, dotted lines indicate the non-existent edges; the green, solid lines indicate the edges we have direct access to and the information about which can be employed to predict the ones indicated by the green, dotted lines; the aim of a link prediction exercise is understanding which of the non-observed links is actually non-existent (indicated by the light blue, dotted lines) and which is genuinely missing (indicated by the light blue, solid lines). Panel **b**: the three subpanels depict a slightly different framework, within which link prediction is carried out by employing node-specific features only - in a way that is reminiscent of network reconstruction exercises [9].

solely concerns these missing edges (see also figure 1). Hereby, we consider algorithms belonging to each of the three, aforementioned classes, such as the Gravity Model (taking as inputs ‘exogenous’ features like each country’s Gross Domestic Product and their geographic distances), the Configuration Model (taking as inputs ‘endogenous’ features like the degrees) and the Gradient Boosting Decision Tree (taking as inputs both ‘exogenous’ and ‘endogenous’ features).

II. SETTING UP THE FRAMEWORK

Let us indicate with \mathbf{A} the $N \times N$ adjacency matrix of the network we are considering, with \mathcal{U} the set of all node pairs and with \mathcal{E} the edge-set: as a consequence, $\mathcal{E}^{ne} = \mathcal{U} \setminus \mathcal{E}$ indicates the set of non-existent links [2, 6]. The edge-set is, then, partitioned into the set of observed, or accessible, links \mathcal{E}^{obs} and the set of missing links $\mathcal{E}^{miss} = \mathcal{E} \setminus \mathcal{E}^{obs}$; lastly, let us denote the union of the set of non-existent links and the set of missing links - collecting the node pairs appearing as unconnected either because the link does not exist or because the information about its presence is missing - as $\mathcal{E}^{no} = \mathcal{E}^{ne} \cup \mathcal{E}^{miss} = \mathcal{U} \setminus \mathcal{E}^{obs}$ [2, 6] (see also the first panel of figure 1a). Link prediction algorithms output $|\mathcal{E}^{no}| = |\mathcal{E}^{ne}| + |\mathcal{E}^{miss}|$ scores to be assigned to the non-observed links: while the $|\mathcal{E}^{miss}|$ largest scores identify the predicted missing links, the remaining $|\mathcal{E}^{ne}|$ scores identify the predicted non-existent ones; let us indicate the two sets as \mathcal{E}^{miss} and \mathcal{E}^{ne} .

A bit more compactly, upon considering that $\mathcal{U} = \mathcal{E}^{obs} \cup \mathcal{E}^{miss} \cup \mathcal{E}^{ne}$, one can define an $N \times N$ adjacency matrix $\mathbf{A}^{obs} = \{a_{ij}^{obs}\}_{(i,j) \in \mathcal{U}}$, where

$$a_{ij}^{obs} = \begin{cases} 1 & \text{if } (i, j) \in \mathcal{E}^{obs} \\ 0 & \text{if } (i, j) \in \mathcal{E}^{miss} \\ 0 & \text{if } (i, j) \in \mathcal{E}^{ne} \end{cases} \quad (1)$$

- in practice, the original matrix \mathbf{A} where $|\mathcal{E}^{miss}|$ connections have been deleted; the *training set*, then, becomes $\mathbf{D}^{tr} = \{\mathbf{X}, \mathbf{A}^{obs}\}$, where $\mathbf{X} = \{\mathbf{x}_{ij}\}_{(i,j) \in \mathcal{U}} = \{\mathbf{f}_i, \mathbf{f}_j, \mathbf{g}_{ij}\}_{(i,j) \in \mathcal{U}}$: as anticipated in the introductory section, the latter is a collection of features, with \mathbf{f}_i and \mathbf{f}_j being the vectors of node-specific features and \mathbf{g}_{ij} being the vector of edge-specific features (see also the second panel of figure 1a). Let us explicitly notice that *i*) ‘endogenous’ features are evaluated on the accessible portion of the dataset \mathbf{A}^{obs} ; *ii*) the structural portion of the training set consists of both connected and unconnected pairs of nodes - as we will see, the main difference between the black-box and white-box algorithms considered here lies precisely in the way such information is processed to make predictions.

After having trained a given model on \mathbf{D}^{tr} , prediction is performed on the *test set*, individuated by the node pairs with no observed connection: in symbols, $\mathbf{D}^{te} = \{a_{ij}\}_{(i,j) \in \mathcal{E}^{no}}$ (see also the third panel of figure 1a).

The goodness of a given prediction performance can be evaluated according to a number of different statistical indicators. Let us indicate the number of true positives (i.e. the correctly identified missing links) with

$$TP = |\overline{\mathcal{E}^{miss}} \cap \mathcal{E}^{miss}|, \quad (2)$$

the number of true negatives with

$$TN = |\overline{\mathcal{E}^{ne}} \cap \mathcal{E}^{ne}| \quad (3)$$

and the number of false positives with

$$FP = |\overline{\mathcal{E}^{miss}} \cap \mathcal{E}^{ne}|; \quad (4)$$

upon doing so, we can define the *True Positives Rate* (TPR) as

$$TPR = \frac{|\overline{\mathcal{E}^{miss}} \cap \mathcal{E}^{miss}|}{|\mathcal{E}^{miss}|}, \quad (5)$$

the *False Positives Rate* (FPR) as

$$FPR = \frac{|\overline{\mathcal{E}^{miss}} \cap \mathcal{E}^{ne}|}{|\mathcal{E}^{ne}|}, \quad (6)$$

the *Jaccard Index* (JI) as

$$JI = \frac{|\overline{\mathcal{E}^{miss}} \cap \mathcal{E}^{miss}|}{|\mathcal{E}^{miss} \cup \mathcal{E}^{miss}|} \quad (7)$$

and the *Accuracy* (ACC) as

$$ACC = \frac{TP + TN}{|\mathcal{E}^{no}|}. \quad (8)$$

In words, the TPR accounts for the percentage of missing links that are correctly identified as such, the JI enriches the picture provided by the TPR by accounting for the number of false positives too and the ACC accounts for the percentage of correctly identified links, be they missing or non-existent. Lastly, the *Area Under the Receiver Operating Curve* (AUROC) is defined as the area under the curve obtained upon scattering the TPR versus the FPR as the list of links ranked in decreasing order of the chosen score is gone through and quantifies the extent to which a given link prediction algorithm performs better than a random one - that flips a coin to classify each non-observed link either as non-existent or missing.

As our link prediction exercise needs the explicit definition of the aforementioned sets and there are many ways of selecting $|\mathcal{E}^{miss}|$ links out of $|\mathcal{E}|$ possible ones, we have randomly selected the 10%, 20%, 30% and 50% of links 10 times to populate \mathcal{E}^{miss} and generate $\mathcal{E}^{obs} = \mathcal{E} \setminus \mathcal{E}^{miss}$; each of the statistical indicators above has, then, been averaged over such samples.

III. MISSING LINKS PREDICTION

Let us, now, illustrate the missing links prediction algorithms considered in the present paper more detailedly.

A. Econometric approaches

A simple, yet successful, recipe to model the World Trade Web (WTW) is the one provided by the Gravity Model (GM) [22, 23]. According to it, the prediction score reads

$$s_{ij}^{\text{GM-I}} = \text{GDP}_i \text{GDP}_j, \quad (9)$$

where GDP_i (GDP_j) is the Gross Domestic Product of country i (country j). A more refined GM-based link prediction recipe reads

$$\begin{aligned} s_{ij}^{\text{GM-II}} &= \ln \left[\epsilon \frac{(\text{GDP}_i \text{GDP}_j)^\beta}{d_{ij}^\gamma} \right] \\ &= \alpha + \beta \ln(\text{GDP}_i \text{GDP}_j) - \gamma \ln d_{ij}, \end{aligned} \quad (10)$$

where d_{ij} is the geographic distance between countries i and j and $\alpha = \ln \epsilon$. To ease numerical manipulations, the GM features have been normalised, thus reading $\omega_i = \text{GDP}_i / \overline{\text{GDP}}$ and $\delta_{ij} = d_{ij} / \bar{d}$, where $\overline{\text{GDP}} = \sum_{i=1}^N \text{GDP}_i / N$ and $\bar{d} = 2 \sum_{i=1}^N \sum_{j(>i)} d_{ij} / (N(N-1))$.

Such a model can be fully determined upon maximising the log-likelihood function

$$\mathcal{L}(\mathbf{A}^{obs} | \alpha, \beta, \gamma) = \sum_{i=1}^N \sum_{j(>i)} [a_{ij}^{obs} \ln p_{ij} + (1 - a_{ij}^{obs}) \ln(1 - p_{ij})], \quad (11)$$

where

$$p_{ij} = \frac{1}{1 + e^{-s_{ij}}}, \quad (12)$$

with $s_{ij} = s_{ij}^{\text{GM-II}}$. In order to evaluate the amount of information required by the recipe above, let us explicitly compute the gradient of the corresponding log-likelihood function. Since

$$\begin{aligned} \mathcal{L}(\mathbf{A}^{obs} | \alpha, \beta, \gamma) &= \sum_{i=1}^N \sum_{j(>i)} [a_{ij}^{obs} \ln(e^{s_{ij}}) - \ln(1 + e^{s_{ij}})] \\ &= \sum_{i=1}^N \sum_{j(>i)} [a_{ij}^{obs} s_{ij} - \ln(1 + e^{s_{ij}})], \end{aligned} \quad (13)$$

one finds

$$\begin{aligned} \frac{\partial \mathcal{L}}{\partial \theta} &= \sum_{i=1}^N \sum_{j(>i)} \left[a_{ij}^{obs} - \frac{e^{s_{ij}}}{1 + e^{s_{ij}}} \right] \frac{\partial s_{ij}}{\partial \theta} \\ &= \sum_{i=1}^N \sum_{j(>i)} [a_{ij}^{obs} - p_{ij}] \frac{\partial s_{ij}}{\partial \theta}, \end{aligned} \quad (14)$$

year	α	β	γ
1990	2.102 ± 0.020	0.436 ± 0.004	0.526 ± 0.009
1991	1.643 ± 0.159	0.409 ± 0.004	0.492 ± 0.007
1992	1.766 ± 0.191	0.425 ± 0.004	0.482 ± 0.009
1993	1.868 ± 0.012	0.443 ± 0.004	0.538 ± 0.013
1994	1.955 ± 0.195	0.442 ± 0.004	0.583 ± 0.028
1995	2.00 ± 0.027	0.442 ± 0.004	0.579 ± 0.015
1996	2.162 ± 0.017	0.449 ± 0.005	0.580 ± 0.016
1997	2.346 ± 0.035	0.472 ± 0.007	0.584 ± 0.016
1998	2.346 ± 0.014	0.474 ± 0.004	0.595 ± 0.019
1999	3.361 ± 0.017	0.477 ± 0.004	0.575 ± 0.015
2000	2.410 ± 0.030	0.486 ± 0.005	0.578 ± 0.017

Table I: Coefficients of the GM-based link prediction recipe defined by eq. 10, trained on the years listed in the first column. The WTW has been considered in its binary, undirected representation.

where $\boldsymbol{\theta} = \{\alpha, \beta, \gamma\}$, an expression showing that the required amount of information coincides with the entire set of observed connections.

The inferred coefficients, obtained by running the scikit-learn Python package [24], are shown in table I.

B. Machine learning approaches

The model we consider here is named Gradient Boosting Decision Tree (GBDT) and belongs to the family of *ensemble methods*, that combine several base-learners, trained in sequence, to achieve a better performance than the one that would be obtained by employing each of them singularly [7, 25, 26]: for binary classification tasks, the GBDT outputs a raw score which is, then, mapped to a probability coefficient. More in detail, the raw score at the K -th step reads

$$s_{ij}^{(K)} = \alpha + \sum_{k=1}^K \rho_{(k)} \phi(\mathbf{x}_{ij} | \boldsymbol{\theta}_{(k)}) \\ = \alpha + \sum_{k=1}^K \rho_{(k)} \phi(\mathbf{f}_i, \mathbf{f}_j, \mathbf{g}_{ij} | \boldsymbol{\theta}_{(k)}), \quad (15)$$

i.e. is a summation over the aforementioned base-learners, parametrised by $\boldsymbol{\theta}$; the parameters ρ and $\boldsymbol{\theta}$ are, then, learnt sequentially. More explicitly, at the zero-th step, one has

$$s_{ij}^{(0)} = \alpha, \quad (16)$$

where the value of α is chosen in order to minimise the loss function (equivalently, maximise the corresponding log-likelihood function)

$$\ell(\mathbf{A}^{obs} | \mathbf{s}^{(0)}) = - \sum_{i=1}^N \sum_{j(>i)} [a_{ij}^{obs} \ln p_{ij} + (1 - a_{ij}^{obs}) \ln(1 - p_{ij})], \quad (17)$$

where $p_{ij} = 1/(1 + e^{-s_{ij}})$. At the first step one has

$$s_{ij}^{(1)} = \alpha + \rho_{(1)} \phi(\mathbf{f}_i, \mathbf{f}_j, \mathbf{g}_{ij} | \boldsymbol{\theta}_{(1)}), \quad (18)$$

where $\boldsymbol{\theta}_{(1)}$ is determined by solving

$$\frac{\partial}{\partial \boldsymbol{\theta}} \left\{ \sum_{i=1}^N \sum_{j(>i)} \left[-\frac{\partial \ell}{\partial s_{ij}} \Big|_{s_{ij}^{(0)}} - \beta \phi(\mathbf{f}_i, \mathbf{f}_j, \mathbf{g}_{ij} | \boldsymbol{\theta}) \right]^2 \right\} = \mathbf{0} \quad (19)$$

or, more explicitly,

$$\sum_{i=1}^N \sum_{j(>i)} \left[-\frac{\partial \ell}{\partial s_{ij}} \Big|_{s_{ij}^{(0)}} - \beta \phi(\mathbf{f}_i, \mathbf{f}_j, \mathbf{g}_{ij} | \boldsymbol{\theta}) \right] \frac{\partial \phi}{\partial \boldsymbol{\theta}} = \mathbf{0}; \quad (20)$$

in words, $\boldsymbol{\theta}$ is chosen to minimise the distance from the gradient of the loss function, evaluated in $s_{ij} = s_{ij}^{(0)}$. Subsequently, $\rho_{(1)}$ is chosen to minimise the ‘updated’ loss function $\ell(\mathbf{A}^{obs} | \mathbf{s}^{(1)})$: by iterating the steps above, it is possible to build a prediction [7].

The base-learners are usually chosen to be *decision trees* [25], hence returning a prediction by performing a sequence of data splits according to the decision rules embodied by the nodes of the trees, with the root corresponding to the initial split and the leaves corresponding to the prediction itself.

The GBDT, trained on a number of different combinations of features - i.e. each country’s GDP, each country’s GDP and their geographic distances, each country’s degree, each country’s degree and their geographic distances - has been implemented by running the LightGBM Python package [26].

C. Entropy-based approaches

Maximum-entropy models have been widely employed, either to detect the empirical patterns of a networked configuration that cannot be interpreted as a mere by-product of the enforced constraints or to individuate the most likely networked configuration(s) that are compatible with the available information: also named *Exponential Random Graphs* (ERGs) [27–33], the models of this class embody a physics-rooted approach to the study of network science [27, 34, 35], ensuring that the imposed constraints are preserved as ensemble averages.

More formally, entropy-based approaches define a probability distribution over a properly-defined ensemble of graphs that is as random as possible, given a set

of M constraints $\mathbf{C}(\mathbf{G}) = \{C_i(\mathbf{G})\}_{i=1}^M$ on the expected value of a number of observables: in symbols,

$$P(\mathbf{G}|\boldsymbol{\theta}) = \frac{e^{-H(\mathbf{G}, \boldsymbol{\theta})}}{Z(\boldsymbol{\theta})} = \frac{e^{-\mathbf{C}(\mathbf{G}) \cdot \boldsymbol{\theta}}}{Z(\boldsymbol{\theta})}, \quad (21)$$

where the parameters $\boldsymbol{\theta}$ are the Lagrange multipliers associated with the constraints themselves. They can be numerically determined by maximising the log-likelihood $\ln P(\mathbf{G}^*|\boldsymbol{\theta})$ of observing the empirical configuration \mathbf{G}^* . It is easy to prove that such a recipe leads to solve the system of non-linear, coupled equations $\langle \mathbf{C} \rangle = \mathbf{C}(\mathbf{G}^*)$, i.e. $\langle C_i \rangle = C_i(\mathbf{G}^*)$, $i = 1 \dots M$ [36–38].

In what follows, we will consider instances of the *separable* Hamiltonian [39]

$$H(\mathbf{A}, \boldsymbol{\theta}) = \sum_{i=1}^N \sum_{j(>i)} H_{ij}(\mathbf{A}, \theta_{ij}) = \sum_{i=1}^N \sum_{j(>i)} a_{ij} \cdot f(\mathbf{A}, \theta_{ij}) \quad (22)$$

that induces a probability distribution reading

$$P(\mathbf{A}|\boldsymbol{\theta}) = \prod_{i=1}^N \prod_{j(>i)} p_{ij}^{a_{ij}} (1 - p_{ij})^{1-a_{ij}} \quad (23)$$

with

$$p_{ij} = \frac{e^{-f(\mathbf{A}, \theta_{ij})}}{1 + e^{-f(\mathbf{A}, \theta_{ij})}}; \quad (24)$$

notice that *linear* Hamiltonians can be recovered as special cases upon posing $f(\mathbf{A}, \theta_{ij}) = f(\theta_{ij})$.

Within such a framework, the $|\mathcal{E}^{miss}|$ largest coefficients of the set $\{p_{ij}\}_{(i,j) \in \mathcal{E}^{no}}$ identify a subgraph Σ^* whose probability reads

$$P(\Sigma^*|\boldsymbol{\theta}) = \prod_i \prod_{j(>i)} p_{ij}^{\sigma_{ij}^*} (1 - p_{ij})^{1-\sigma_{ij}^*}, \quad (25)$$

the product running over the pairs of nodes in \mathcal{E}^{no} and σ_{ij}^* being 1 only for the (i, j) s corresponding to the $|\mathcal{E}^{miss}|$ largest probability coefficients - the remaining entries reading zero: among all subgraphs induced by precisely $|\mathcal{E}^{miss}|$ links, Σ^* is the one attaining the highest probability. In words, entropy-based methods lead us to interpret the non-observed links which have been assigned the largest probability coefficients as the ones that are most likely to appear given the chosen constraints [6].

1. Link prediction via linear ERGs

Configuration Model. Let us, now, consider the first specification of the entropy-based framework: it boils down

to posing $\mathbf{C} = \mathbf{k}$, with $k_i = \sum_{j(\neq i)} a_{ij}$, an identification that leads to $H_{CM}(\mathbf{A}) = \sum_{i=1}^N \sum_{j(>i)} a_{ij} \cdot (\theta_i + \theta_j)$, further inducing

$$p_{ij}^{CM} = \frac{x_i x_j}{1 + x_i x_j}, \quad (26)$$

where $x_i = e^{-\theta_i}$; the parameters $\{x_i\}_{i=1}^N$ can be determined by solving the system of non-linear, coupled equations

$$k_i(\mathbf{A}^{obs}) = \sum_{j(\neq i)} p_{ij}^{CM} = \sum_{j(\neq i)} \frac{x_i x_j}{1 + x_i x_j}, \quad \forall i, \quad (27)$$

a task that can be accomplished by implementing the iterative recipe [37]

$$x_i^{t+1} = \frac{k_i(\mathbf{A}^{obs})}{\sum_{j(\neq i)} \left(\frac{x_j^t}{1 + x_i^t x_j^t} \right)}. \quad (28)$$

The prescription above, characterising the so-called *Configuration Model* (CM) [27, 29–31, 33], matches the one considered in [6], where the accessible portion of a graph was employed to estimate its degree sequence and, on this basis, obtain the probability for any two nodes to be connected - to be later employed as a score for the existence of a link between any two unconnected vertices. Such a procedure rests upon the assumption that if the accessible portion of a graph is reproduced with a certain accuracy by a certain topological information, the inaccessible portion will be reproduced with the same degree of accuracy by the same kind of information¹.

A simpler prescription ensuring that the expected degree sequence matches the observed one is provided by the Chung-Lu model (CL):

$$p_{ij}^{CL} = \frac{k_i k_j}{2L}, \quad (29)$$

where k_i and k_j must be interpreted as the degrees of the nodes evaluated on the accessible portion of the dataset \mathbf{A}^{obs} , i.e. $k_i(\mathbf{A}^{obs})$ and $k_j(\mathbf{A}^{obs})$; as it can be recovered from the CM by posing $p_{ij}^{CM} \simeq x_i x_j$, the validity of this model is limited to the case in which the network is sparse and the degree distribution is not too broad [37].

¹ In a sense, the link prediction problem is interpreted as an instance of the network reconstruction one [1, 40], the aim of which is precisely that of inferring a graph structure from a set of observed quantities - although network reconstruction usually deals with *less information* to predict *more aggregate* properties (see also figure 1b).

Configuration Model with Distances. Let us, now, enrich the CM by adding information about the geographic distances between countries: this choice boils down to posing $\mathbf{C} = \{\mathbf{k}, d\}$, with $k_i = \sum_{j(\neq i)} a_{ij}$ and $d = \sum_{i=1}^N \sum_{j(>i)} a_{ij} d_{ij}$ [41, 42]. Such an identification leads to $H_{\text{CMD}}(\mathbf{A}) = \sum_{i=1}^N \sum_{j(>i)} a_{ij} \cdot (\theta_i + \theta_j + \gamma d_{ij})$, an expression inducing

$$p_{ij}^{\text{CMD}} = \frac{x_i x_j w^{d_{ij}}}{1 + x_i x_j w^{d_{ij}}}, \quad (30)$$

where $x_i = e^{-\theta_i}$ and $w = e^{-\gamma}$. The parameters $\{x_i\}_{i=1}^N$ and w can be determined by solving the system of non-linear, coupled equations

$$\begin{cases} k_i(\mathbf{A}^{\text{obs}}) = \sum_{j(\neq i)} p_{ij}^{\text{CMD}}, \quad \forall i \\ d(\mathbf{A}^{\text{obs}}) = \sum_{i=1}^N \sum_{j(>i)} p_{ij}^{\text{CMD}} d_{ij} \end{cases} \quad (31)$$

a task that can be accomplished by implementing the iterative recipe

$$\begin{cases} x_i^{t+1} = \frac{k_i(\mathbf{A}^{\text{obs}})}{\sum_{j(\neq i)} \left(\frac{x_j^t w_t^{d_{ij}}}{1 + x_i^t x_j^t w_t^{d_{ij}}} \right)}, \quad \forall i \\ w_{t+1} = \frac{d(\mathbf{A}^{\text{obs}})}{\sum_{i=1}^N \sum_{j(>i)} \left(\frac{x_i^t x_j^t w_t^{d_{ij}-1}}{1 + x_i^t x_j^t w_t^{d_{ij}}} \right) d_{ij}} \end{cases} \quad (32)$$

notice how the *Configuration Model with Distances* (CMD) relies upon both ‘endogenous’ (i.e. topological) and ‘exogenous’ (i.e. non-topological) features. To ease numerical manipulations, the distances have been normalised, thus reading $\delta_{ij} = d_{ij}/\bar{d}$, where $\bar{d} = 2 \sum_{i=1}^N \sum_{j(>i)} d_{ij}/N(N-1)$.

Fitness Model. Firstly introduced in [43] as a generative mechanism alternative to the ‘rich-gets-richer’ one, the *Fitness Model* (FM) prescribes to associate each node with a hidden variable: following [44], here we pose $x_i = \sqrt{z} \omega_i$, with $\omega_i = \text{GDP}_i/\overline{\text{GDP}}$ and $\overline{\text{GDP}} = \sum_{i=1}^N \text{GDP}_i/N$, thus obtaining

$$p_{ij}^{\text{FM}} = \frac{z \omega_i \omega_j}{1 + z \omega_i \omega_j}. \quad (33)$$

The parameter z can be inferred by imposing that the expected number of links matches the observed one $L(\mathbf{A}^{\text{obs}}) = |\mathcal{E}^{\text{obs}}|$, i.e. that

$$L(\mathbf{A}^{\text{obs}}) = \sum_{i=1}^N \sum_{j(>i)} p_{ij}^{\text{FM}}, \quad (34)$$

a task that can be accomplished by implementing the iterative recipe

$$z_{t+1} = \frac{L(\mathbf{A}^{\text{obs}})}{\sum_{i=1}^N \sum_{j(>i)} \left(\frac{\omega_i \omega_j}{1 + z_t \omega_i \omega_j} \right)}. \quad (35)$$

A different position reads $x_i = \sqrt{z} s_i$, where, now, $s_i = \sum_{j(\neq i)} w_{ij}$ indicates the strength of node i . This second choice is a popular one when analysing financial networks, the available data about which usually concern lending and borrowing relationships. This second specification is also known with the name of *density-corrected Gravity Model* (dcGM) [40, 45].

Fitness Model with Distances. As for the CM, also the CMD can be turned into a *Fitness Model with Distances* (FMD). By operating the same replacement as above, one gets

$$p_{ij}^{\text{FMD}} = \frac{z \omega_i \omega_j w^{d_{ij}}}{1 + z \omega_i \omega_j w^{d_{ij}}}, \quad (36)$$

the system to be solved, now, reading

$$\begin{cases} L(\mathbf{A}^{\text{obs}}) = \sum_{i=1}^N \sum_{j(>i)} p_{ij}^{\text{FMD}} \\ d(\mathbf{A}^{\text{obs}}) = \sum_{i=1}^N \sum_{j(>i)} p_{ij}^{\text{FMD}} d_{ij} \end{cases} \quad (37)$$

and the iterative recipe becoming

$$\begin{cases} z_{t+1} = \frac{L(\mathbf{A}^{\text{obs}})}{\sum_{i=1}^N \sum_{j(>i)} \left(\frac{\omega_i \omega_j w^{d_{ij}}}{1 + z_t \omega_i \omega_j w^{d_{ij}}} \right)} \\ w_{t+1} = \frac{d(\mathbf{A}^{\text{obs}})}{\sum_{i=1}^N \sum_{j(>i)} \left(\frac{z_t \omega_i \omega_j w_t^{d_{ij}-1}}{1 + z_t \omega_i \omega_j w_t^{d_{ij}}} \right) d_{ij}} \end{cases} \quad (38)$$

To ease numerical manipulations, the distances have been normalised, thus reading $\delta_{ij} = d_{ij}/\bar{d}$, where $\bar{d} = 2 \sum_{i=1}^N \sum_{j(>i)} d_{ij}/N(N-1)$.

2. Link prediction via non-linear ERGs

So far, we have focused on linear ERGs; let us, now, move to considering non-linear ERGs.

Fitness-induced 2-Star Model. The simplest model of this kind is the so-called *2-Star Model* (2SM) [27, 46, 47], induced by posing $\mathbf{C} = \{L, S\}$, with

$L = \sum_{i=1}^N \sum_{j(>i)} a_{ij} = \sum_{i=1}^N k_i/2$ and $S = \sum_{i=1}^N \sum_{j(>i)} \sum_{m(\neq i,j)} a_{im} a_{mj} = \sum_{i=1}^N k_i^2/2 - L$. Such an identification leads to $H_{2\text{SM}}(\mathbf{A}) = \sum_{i=1}^N \sum_{j(>i)} a_{ij} \cdot [\alpha + \beta(k_i + k_j)]$, an expression inducing

$$p_{ij}^{\text{2SM}} = \frac{xy^{\langle k_i \rangle + \langle k_j \rangle}}{1 + xy^{\langle k_i \rangle + \langle k_j \rangle}}, \quad (39)$$

where $x = e^{-\alpha}$ and $y = e^{-\beta}$. One would be tempted to identify the expected value of the degrees with the observed one but consistency forbids such a match: as the only available information concerns two, global quantities, degrees are not directly accessible. In order to make the model fully consistent, a more refined formulation is, thus, needed.

First, the model we are looking for should be heterogeneous, thus ensuring that node-specific differences are preserved. More quantitatively, one would be looking for an expression like

$$p_{ij}^{\text{dc2SM}} = \frac{x_i x_j y^{k_i + k_j}}{1 + x_i x_j y^{k_i + k_j}}, \quad (40)$$

where k_i and k_j must be interpreted as the degrees of the nodes evaluated on \mathbf{A}^{obs} , i.e. $k_i(\mathbf{A}^{\text{obs}})$ and $k_j(\mathbf{A}^{\text{obs}})$; as proven in [39], however, the model above, named *degree-corrected 2-Star Model* (dc2SM), suffers from limitations inherited by the mean-field approach inducing it. One is, thus, forced to consider a fitness-based variant of it, reading either

$$p_{ij}^{\text{fit2SM-I}} = \frac{z \omega_i \omega_j y^{\langle k_i \rangle + \langle k_j \rangle}}{1 + z \omega_i \omega_j y^{\langle k_i \rangle + \langle k_j \rangle}}, \quad (41)$$

where $\langle k_i \rangle = \sum_{j(\neq i)} p_{ij}^{\text{fit2SM-I}}$, or

$$p_{ij}^{\text{fit2SM-II}} = \frac{z s_i s_j y^{\langle k_i \rangle + \langle k_j \rangle}}{1 + z s_i s_j y^{\langle k_i \rangle + \langle k_j \rangle}}, \quad (42)$$

where $\langle k_i \rangle = \sum_{j(\neq i)} p_{ij}^{\text{fit2SM-II}}$. A third variant can be defined as

$$p_{ij}^{\text{fit2SM-III}} = \frac{z \tilde{x}_i \tilde{x}_j y^{\langle k_i \rangle + \langle k_j \rangle}}{1 + z \tilde{x}_i \tilde{x}_j y^{\langle k_i \rangle + \langle k_j \rangle}}, \quad (43)$$

where $\langle k_i \rangle = \sum_{j(\neq i)} \tilde{x}_i \tilde{x}_j / (1 + \tilde{x}_i \tilde{x}_j) = k_i$; the major difference with respect to the first recipe is the disentangled resolution of the formula above: in other words, one, first, determines the parameters $\{\tilde{x}_i\}_{i=1}^N$ by solving the CM and, then, insert them above to determine z and y .

The difference with respect to the 2SM is evident: the three variants above are heterogeneous, hence likely reproducing the observed degrees better than the 2SM. The

parameters z and y can be determined by solving the system of non-linear, coupled equations

$$\begin{cases} L(\mathbf{A}^{\text{obs}}) = \sum_{i=1}^N \sum_{j(>i)} p_{ij}^{\text{fit2SM}} \\ S(\mathbf{A}^{\text{obs}}) = \sum_{i=1}^N \sum_{j(>i)} \sum_{m(\neq i,j)} p_{im}^{\text{fit2SM}} p_{mj}^{\text{fit2SM}} \end{cases} \quad (44)$$

where we have dropped the reference to the model specification as the recipe is the same in all cases.

Let us, now, face the problem of determining the expected degrees; to this aim, let us focus on the third recipe: as the parameters $\{\tilde{x}_i\}_{i=1}^N$ have been determined by solving the CM on \mathbf{A}^{obs} , we can insert the observed degrees directly into the recipe above. As a consequence, the two parameters z and y can, now, be obtained by implementing the iterative recipe

$$\begin{cases} z_{t+1} = \frac{L(\mathbf{A}^{\text{obs}})}{\sum_{i=1}^N \sum_{j(>i)} \frac{\tilde{x}_i \tilde{x}_j y_t^{k_i + k_j}}{1 + z_t \tilde{x}_i \tilde{x}_j y_t^{k_i + k_j}}} \\ y_{t+1} = \frac{S(\mathbf{A}^{\text{obs}})}{\sum_{i=1}^N \sum_{j(>i)} \sum_{m(\neq i,j)} \frac{z_t^2 \tilde{x}_i \tilde{x}_m y_t^{k_i + 2k_m + k_j - 1}}{(1 + z_t \tilde{x}_i \tilde{x}_m y_t^{k_i + k_m})(1 + z_t \tilde{x}_m \tilde{x}_j y_t^{k_m + k_j})}} \end{cases} \quad (45)$$

where k_i , k_m and k_j must be interpreted as the degrees of the nodes evaluated on the accessible portion of the dataset \mathbf{A}^{obs} , i.e. $k_i(\mathbf{A}^{\text{obs}})$, $k_m(\mathbf{A}^{\text{obs}})$ and $k_j(\mathbf{A}^{\text{obs}})$.

III. DATA DESCRIPTION

The aforementioned link prediction algorithms have been run and compared on a number of instances of economic and financial datasets.

As a first dataset, we have considered the WTW curated by Gleditsch [48] and including yearly, bilateral, aggregated data on trade (the generic entry $\exp_{ij}(y)$ is the sum of the single, commodity-specific exports from i to j , during the year y , reported in millions of US dollars), yearly GDP values (reported in millions of US dollars) and the (time-independent) matrix of geographic distances between the capital cities of the countries in the data. We have, then, symmetrised and binarised the trade matrix by posing $a_{ij} = \Theta[w_{ij}]$, where Θ is the Heaviside step function and $w_{ij} = (\exp_{ij} + \exp_{ji})/2$ - in words, w_{ij} is the bilateral trade volume defined as the arithmetic mean of the export volume from country i to country j and the export volume from country j to country i - for each of the eleven years going from 1990 to 2000.

year	N	L	c	\bar{k}
1990	159	7639	0.608	96.08
1991	173	8249	0.554	95.36
1992	175	8552	0.562	97.74
1993	177	8837	0.567	99.85
1994	177	9052	0.591	103.94
1995	177	9199	0.591	103.94
1996	177	9623	0.618	108.73
1997	177	9864	0.633	111.46
1998	177	9866	0.633	111.48
1999	177	9864	0.633	111.46
2000	177	9865	0.633	111.47

Table II: Basic statistics concerning the WTW dataset [48], i.e. the total number of countries N , the total number of links L , the network density c and the average degree \bar{k} .

As a second dataset, we have considered the electronic Market for Interbank Deposit (eMID) [39], represented as a weighted, directed network whose nodes are anonymised banks and weights represent exposures in millions of euros. Reported data cover the period January 1999-December 2014 on a daily frequency: the presence of a weight w_{ij} at time t indicates the existence of a total exposure $w_{ij} \geq 50.000$ euros, registered at the end of the particular period t and directed from bank i to bank j . Considering that $\simeq 98\%$ of banks are Italian and that the volume of their transactions covers $\simeq 85\%$ of the total volume (as of 2011), our analysis solely focuses on the subgraph induced by such a subset of nodes. We have, then, symmetrised and binarised the exposure matrix by posing $a_{ij} = \Theta[w_{ij} + w_{ji}]$ - in words, $w_{ij} + w_{ji}$ is the sum of the exposures of the involved banks - for each aggregation period ranging from daily to yearly.

IV. RESULTS

As in a real-case scenario the choice between different methods would be determined by the available features, it is useful to compare models informed by the same quantities. To this aim, let us recall that *i*) the GM, defined by eq. 10, takes as inputs the GDPs and the geographic distances; *ii*) the first formulation of the FM, defined by eq. 33, takes as inputs the GDPs; *iii*) the second formulation of the FM, defined by eq. 36, takes as inputs the GDPs and the geographic distances; *iv*) the CM and the CL, respectively defined by eqs. 26 and 29, take as inputs the degrees; *v*) the CMD, defined by eq. 30, takes as inputs the degrees and the geographic distances; *vi*) the fit2SM, defined by eq. 43, takes as inputs the degrees (as the total number of links and the total number of two-stars can be deduced from them). Naturally, we have compared the performance of each white-box method with the instance of the GBDT taking

year	N	L	c	\bar{k}
1999	215	9770	0.424	90.88
2000	195	8172	0.432	83.81
2001	182	6669	0.401	73.29
2002	176	5528	0.359	62.82
2003	176	4892	0.318	55.59
2004	175	4327	0.284	49.45
2005	172	4119	0.280	47.90
2006	172	3910	0.266	45.47
2007	170	3886	0.270	45.72
2008	157	3161	0.258	40.27
2009	137	2381	0.256	34.76
2010	127	2192	0.274	34.52
2011	112	2036	0.328	36.36
2012	97	1421	0.306	29.30

Table III: Basic statistics concerning the eMID dataset [39], aggregated at the yearly level. The table shows the total number of banks N , the total number of links L , the network density c and the average degree \bar{k} .

as input the same amount of information.

Let us start commenting on the WTW. The basic statistics are reported in table II: as it can be appreciated, the number of nodes N ranges between 159 and 177 and the total number of links L ranges between 7639 and 9866; still, the link density $c = 2L/N(N - 1)$ does not fluctuate much, ranging between 0.55 and 0.63, as well as the average degree $\bar{k} = 2L/N$, ranging between $\gtrsim 95$ and $\gtrsim 111$.

Figure 2 depicts the TPR for each of the aforementioned models, on the years 1990, 1995 and 2000. Let us recall that it is defined as $\text{TPR} = |\overline{\mathcal{E}}^{\text{miss}} \cap \mathcal{E}^{\text{miss}}| / |\overline{\mathcal{E}}^{\text{miss}}|$, hence accounting for the percentage of missing links that are correctly identified as such. First, let us notice that when considering ‘exogenous’ features, each instance of the GBDT outperforms its white-box counterpart. The two classes of models, instead, perform in a comparable way when coming to consider ‘endogenous’ features such as the degrees and the number of two-stars: quite interestingly, the CL is the method performing worst, while the CM and the fit2SM perform in a very similar way - a result indicating that the present application does not necessarily require to consider non-linear ERGs. The white-box model performing best, and outperforming the corresponding instance of the GBDT, is the CMD, taking as input a combination of ‘endogenous’ and ‘exogenous’ features.

Figure 3 depicts $\text{JI} = |\overline{\mathcal{E}}^{\text{miss}} \cap \mathcal{E}^{\text{miss}}| / |\overline{\mathcal{E}}^{\text{miss}} \cup \mathcal{E}^{\text{miss}}|$, hence enriching the picture provided by the TPR by accounting for the number of false positives too; figure 4 depicts $\text{ACC} = (\text{TP} + \text{TN}) / |\mathcal{E}^{\text{no}}|$ for each of the aforementioned models, hence accounting for the percentage of correctly identified links, be they missing or non-existent: both return a picture that is consistent with the one re-

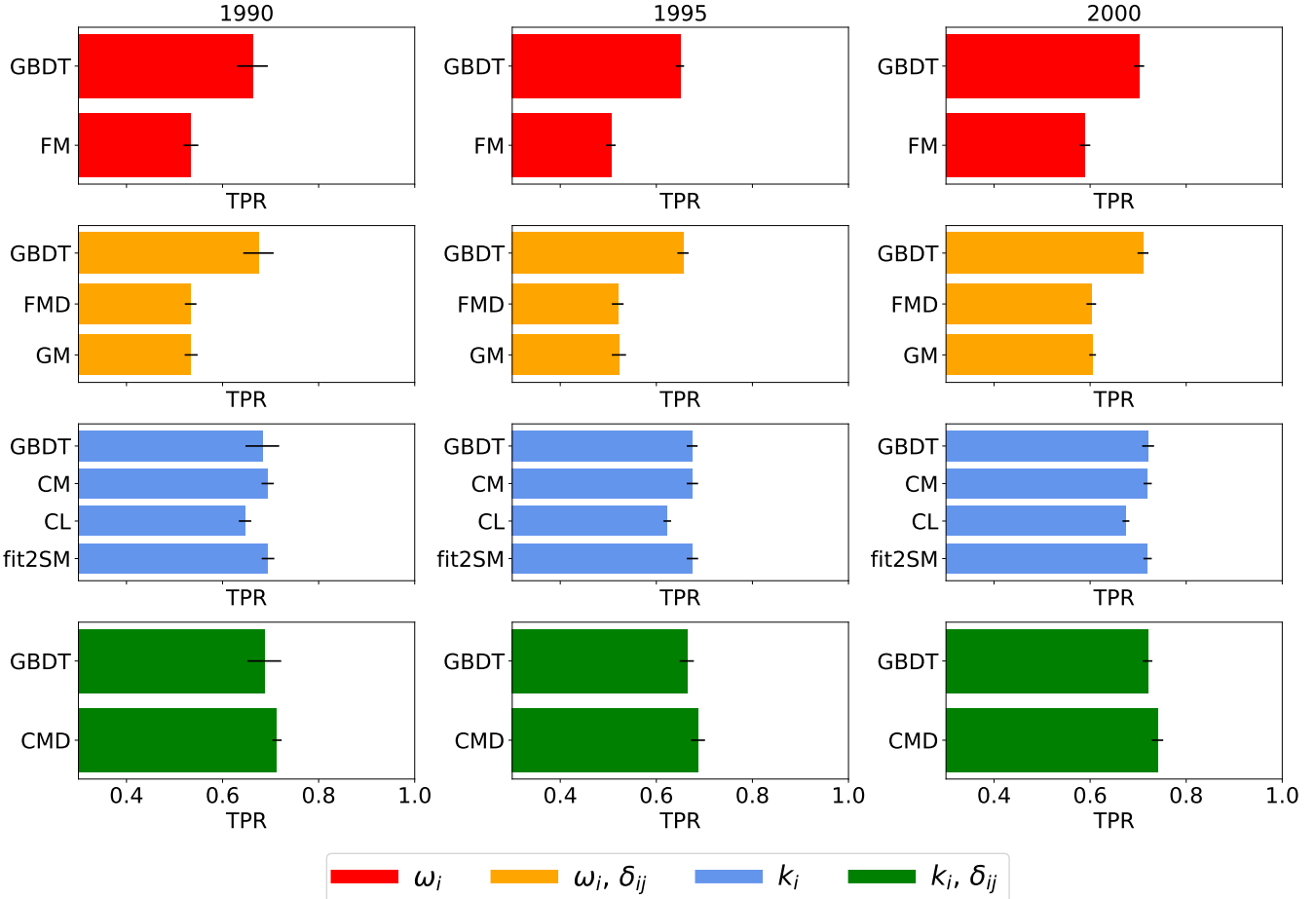


Figure 2: Performance of the models, measured in terms of TPR, for the years 1990, 1995 and 2000 of the WTW. Each panel collects methods that rely on the same set of features (see the colour legend). The upper bar in each panel, marked with a diagonal pattern, corresponds to the black-box GBDT. We have randomly selected the 10% of links 10 times to populate \mathcal{E}^{miss} and generate $\mathcal{E}^{obs} = \mathcal{E} \setminus \mathcal{E}^{miss}$; each statistical indicator has, then, been averaged over such samples, the standard deviation being represented by a horizontal, black bar. When considering ‘exogenous’ features, each instance of the GBDT outperforms its white-box counterpart. The two classes of models, instead, perform in a comparable way when coming to consider ‘endogenous’ features such as the degrees. The only white-box model outperforming the corresponding instance of the GBDT is the CMD, taking as input a combination of ‘endogenous’ and ‘exogenous’ features, i.e. the degrees and the geographic distances.

turned by the TPR.

A complementary picture is provided by figure 5, showing the ROC curves, obtained upon scattering the $TPR = |\mathcal{E}^{miss} \cap \mathcal{E}^{miss}| / |\mathcal{E}^{miss}|$ versus the $FPR = |\mathcal{E}^{miss} \cap \mathcal{E}^{ne}| / |\mathcal{E}^{ne}|$ as the list of links ranked in decreasing order of the chosen score is gone through, for each of the aforementioned models, on the years 1990, 1995 and 2000. As evident upon looking at the picture, the AUROC of white-box models enlarges when moving from less structured models like the GM to more structured ones like the CMD.

All the aforementioned exercises have been carried out by randomly selecting the 10% of links 10 times to populate \mathcal{E}^{miss} and generate $\mathcal{E}^{obs} = \mathcal{E} \setminus \mathcal{E}^{miss}$ - each

statistical indicator has, then, been averaged over such samples: the results we have obtained for a different percentage of randomly selected links are shown in Appendix A. As it can be appreciated, the performance of the CMD remains high up to a large percentage of removed connections - equivalently, of missing links; still, the performance of the GBDT deteriorates to a lesser extent than the one of white-box models.

Let us, now, move to commenting on eMID, aggregated at the yearly level as well. The basic statistics are reported in table III: as it can be appreciated, the number of nodes N ranges between 97 and 215 and the total number of links L ranges between 1421 and 9770; the link

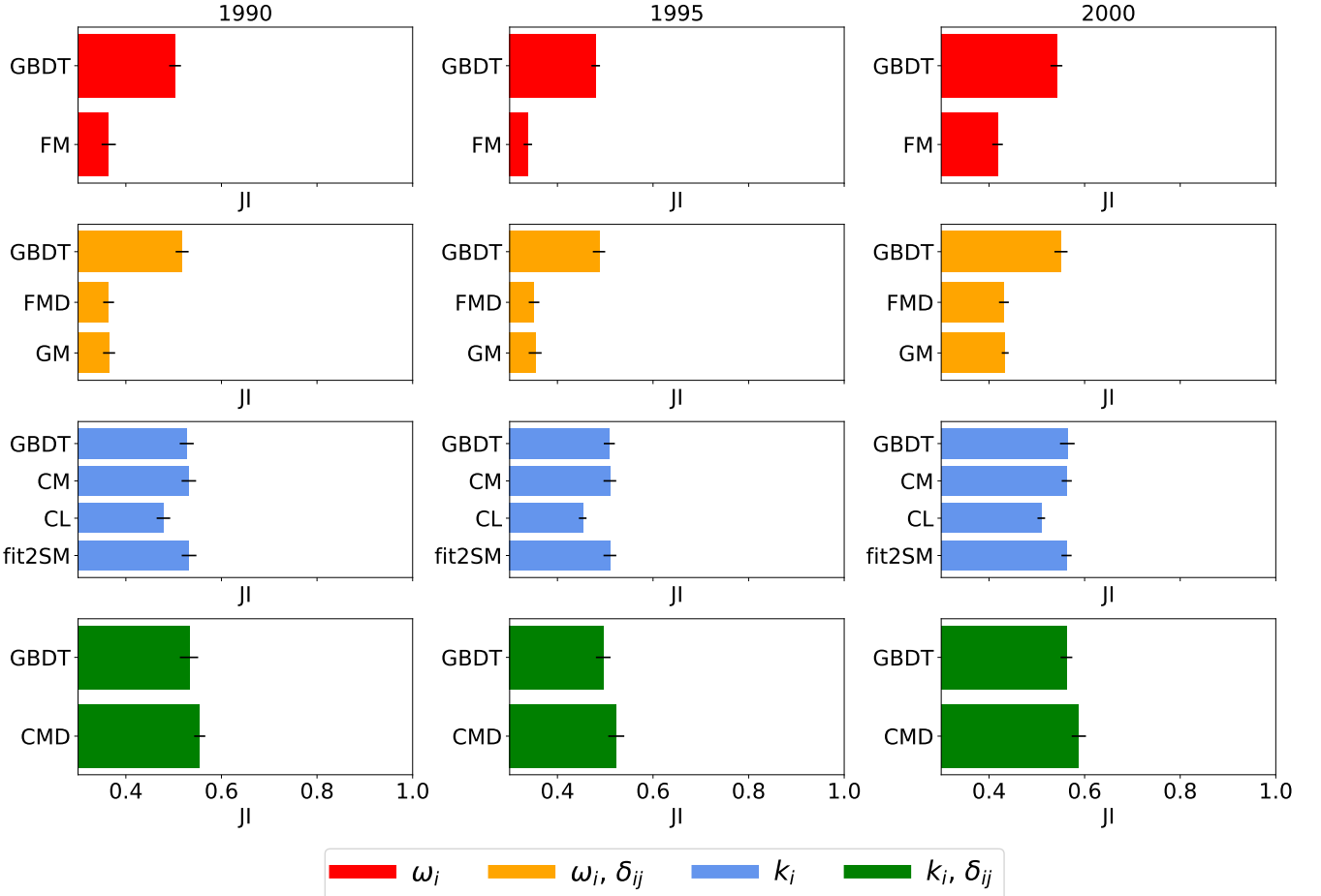


Figure 3: Performance of the models, measured in terms of JI, for the years 1990, 1995 and 2000 of the WTW. Each panel collects methods that rely on the same set of features (see the colour legend). The upper bar in each panel, marked with a diagonal pattern, corresponds to the black-box GBDT. We have randomly selected the 10% of links 10 times to populate \mathcal{E}^{miss} and generate $\mathcal{E}^{obs} = \mathcal{E} \setminus \mathcal{E}^{miss}$; each statistical indicator has, then, been averaged over such samples, the standard deviation being represented by a horizontal, black bar. When considering ‘exogenous’ features, each instance of the GBDT outperforms its white-box counterpart. The two classes of models, instead, perform in a comparable way when coming to consider ‘endogenous’ features such as the degrees. The only white-box model outperforming the corresponding instance of the GBDT is the CMD, taking as input a combination of ‘endogenous’ and ‘exogenous’ features, i.e. the degrees and the geographic distances.

density $c = 2L/N(N-1)$ fluctuates appreciably between 0.26 and 0.43, as well as the average degree $k = 2L/N$, ranging between $\gtrsim 29$ and $\lesssim 91$. As, in this case, no external feature is available a priori, we have excluded comparisons of the kind.

All results are shown in figure 6. Overall, the larger sparsity of the system under consideration leads to TPR and JI scores that are lower than the ones obtained when analysing the WTW; in the case of eMID, in fact, reproducing the 1s is (much) more difficult than reproducing the 0s: as a consequence, a (much) worse performance on the number of true positives than on the number of true negatives is expected. As for the WTW, however, each ‘endogenous’ instance of the GBDT performs in a way

that is comparable to the one of its purely structural, white-box counterpart, especially for what concerns the CM and the fit2SM - although the sparsity of eMID lets the CL perform as well as the CM and the fit2SM.

All the aforementioned exercises on eMID have been carried out by randomly selecting the 20% of links 10 times to populate \mathcal{E}^{miss} and generate $\mathcal{E}^{obs} = \mathcal{E} \setminus \mathcal{E}^{miss}$ - each statistical indicator has, then, been averaged over such samples: the results we have obtained for a different aggregation level are shown in Appendix B. As can be appreciated, very similar results to the ones characterising the yearly aggregation level are obtained.

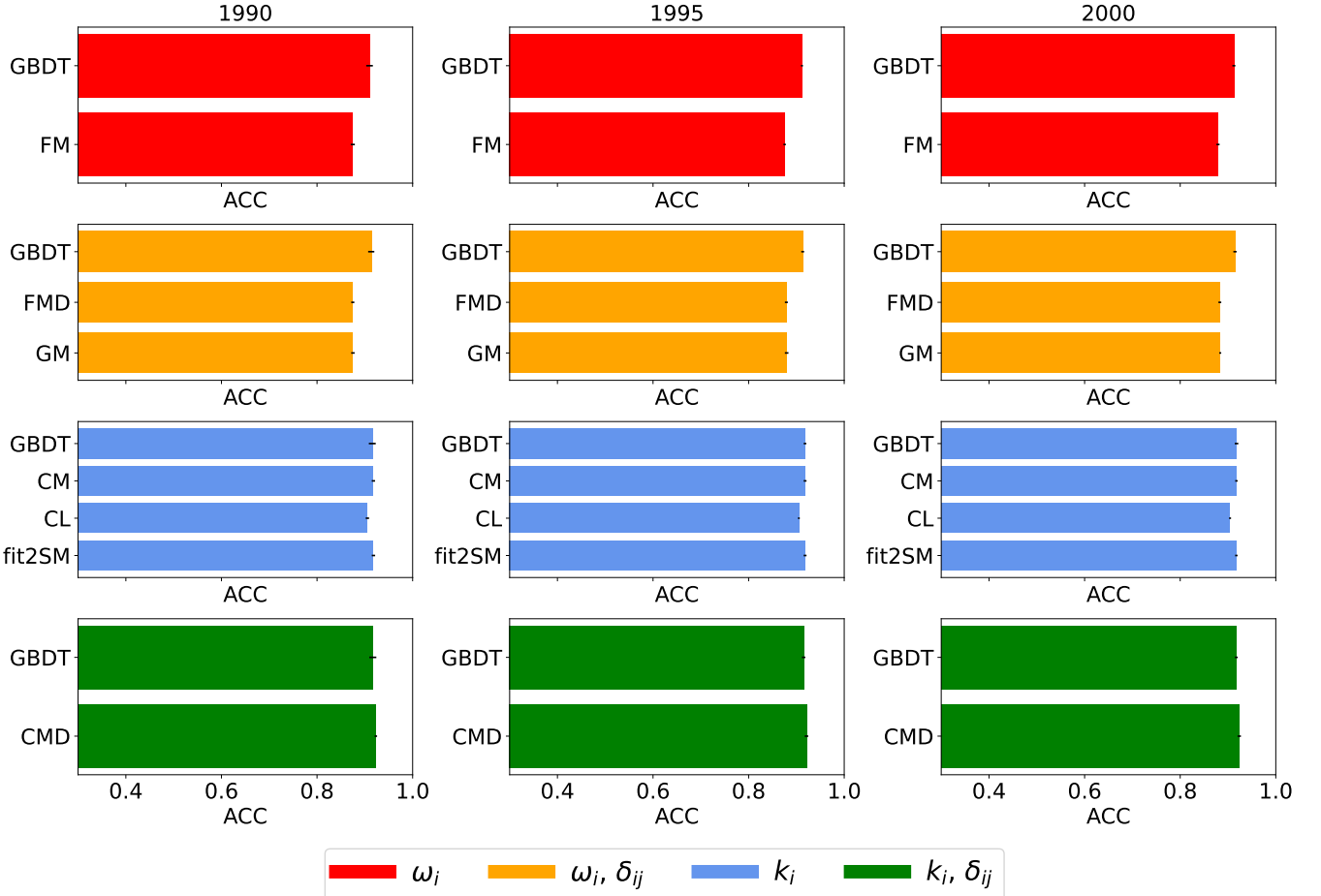


Figure 4: Performance of the models, measured in terms of ACC, for the years 1990, 1995 and 2000 of the WTW. Each panel collects methods that rely on the same set of features (see the colour legend). The upper bar in each panel, marked with a diagonal pattern, corresponds to the black-box GBDT. We have randomly selected the 10% of links 10 times to populate \mathcal{E}^{miss} and generate $\mathcal{E}^{obs} = \mathcal{E} \setminus \mathcal{E}^{miss}$; each statistical indicator has, then, been averaged over such samples, the standard deviation being represented by a horizontal, black bar. When considering ‘exogenous’ features, each instance of the GBDT outperforms its white-box counterpart. The two classes of models, instead, perform in a comparable way when coming to consider ‘endogenous’ features such as the degrees. The only white-box model outperforming the corresponding instance of the GBDT is the CMD, taking as input a combination of ‘endogenous’ and ‘exogenous’ features, i.e. the degrees and the geographic distances.

V. DISCUSSION

The aim of the present contribution is that of comparing the performance of several algorithms in carrying out a link prediction exercise. In order to do so, we pose ourselves in the same setting of [2, 6], where the variables of interest are computed on the observed portion of the graph (i.e. \mathbf{A}^{obs}) and the prediction is carried out on the pairs of nodes in \mathcal{E}^{no} , which correspond to the entries $a_{ij}^{obs} = 0, \forall (i, j) \in \mathcal{E}^{no}$, hence appearing as not connected.

Within such a framework, the best performance is obtained when the purely structural information is combined with the available, external information: for what

concerns the WTW, the latter consists of two sets of properties, i.e. the GDPs of countries and the geographic distances between them; while, however, the FMD does not perform better than the FM and the GM, enriching the CM with the information concerning the geographic distances leads to a better performance than the one characterising the GBDT taking as inputs the same sets of quantities.

Such a result leads us to the conclusion that the structural information plays a fundamental role in shaping a network topology: it is, in fact, so relevant to make the CM alone capable of competing with the instance of the GBDT taking as inputs the degrees; in other words, although machine learning algorithms appear as among

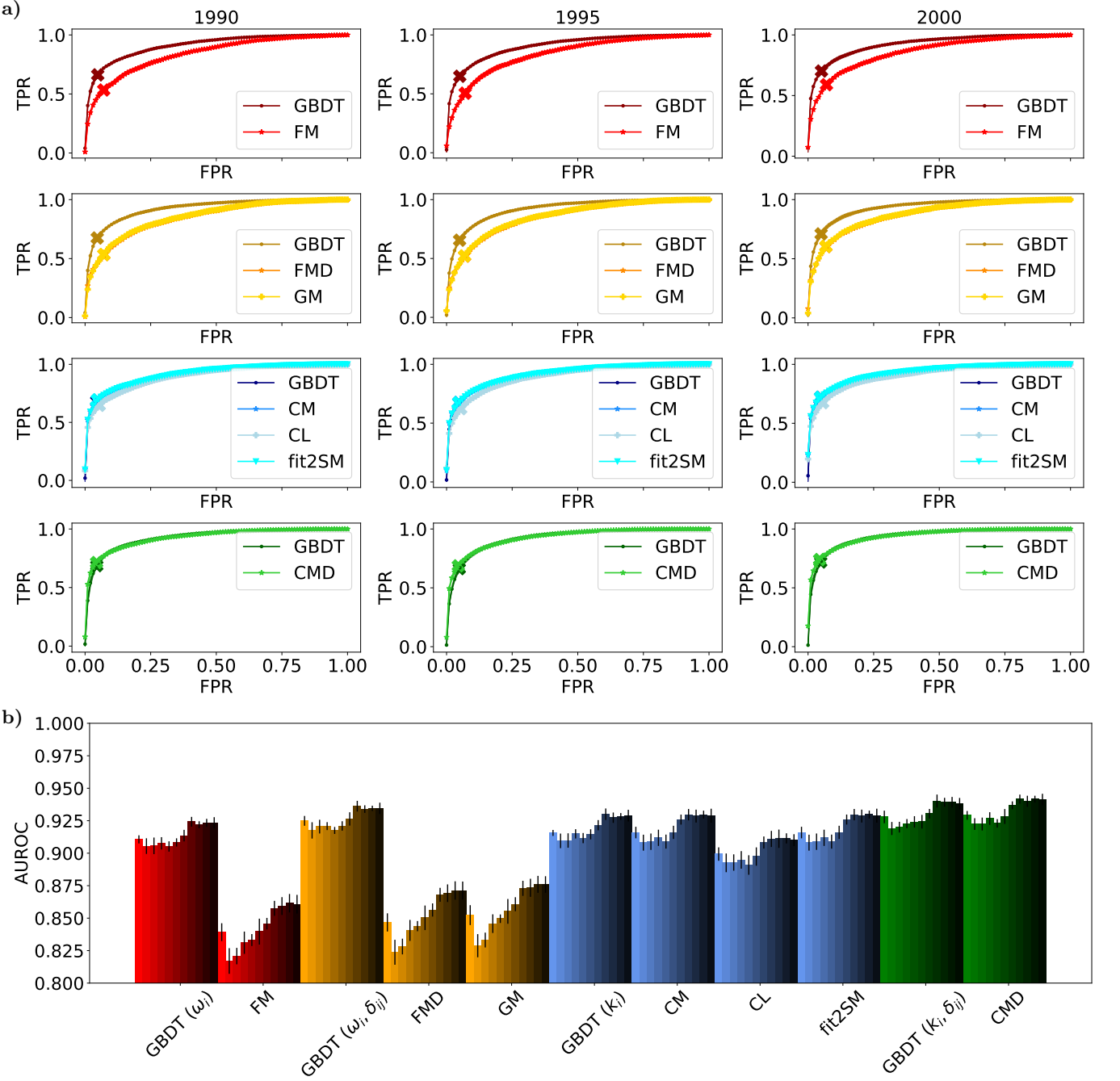


Figure 5: Panels a: performance of the models, measured in terms of ROC curves, for the years 1990, 1995 and 2000 of the WTW. Each panel collects methods that rely on the same set of features. We have randomly selected the 10% of links 10 times to populate \mathcal{E}^{miss} and generate $\mathcal{E}^{obs} = \mathcal{E} \setminus \mathcal{E}^{miss}$ (the curves relative to each indicator are, in fact, 10 partially overlapping curves corresponding to each realization). The 'X' markers indicate the TPR and FPR values obtained by selecting a number of missing links equal to $|\mathcal{E}^{miss}|$. Panel b: each statistical indicator has been averaged over the 10 realizations sample, the standard deviation being represented by a vertical, black bar. The AUROC, depicted for all years (darker shades correspond to more recent years), enlarges when moving from less structured models, like the GM, to more structured ones, like the CMD.

those performing best, white-box models taking as inputs purely ‘endogenous’ features offer a comparable - in some

cases, even slightly superior - performance. This is even more relevant when considering that the GBDT needs a

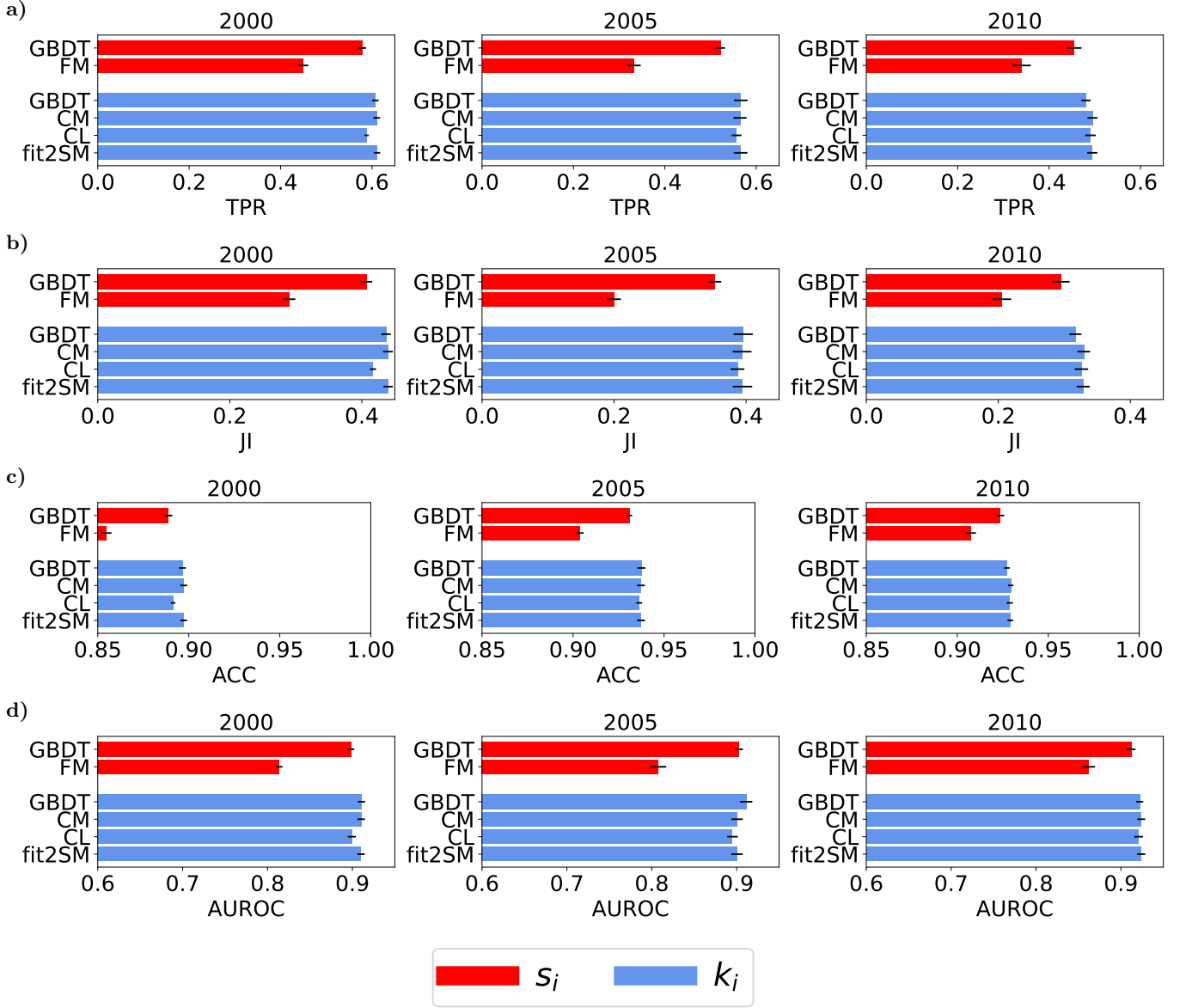


Figure 6: Performance of the models, measured in terms of TPR (row a), JI (row b), ACC (row c) and AUROC (row d), for the years 2000, 2005 and 2010 of eMID. The upper bar in each panel, marked with a diagonal pattern, corresponds to the black-box GBDT. We have randomly selected the 20% of links 10 times to populate \mathcal{E}^{miss} and generate $\mathcal{E}^{obs} = \mathcal{E} \setminus \mathcal{E}^{miss}$; each statistical indicator has, then, been averaged over such samples, the standard deviation being represented by a horizontal, black bar. The FM has been implemented by replacing ω_i with s_i in eq. 33 (see the colour legend). As for the WTW, each ‘endogenous’ instance of the GBDT performs in a way that is comparable to that of its purely structural, white-box counterparts - especially for what concerns the CM and the fit2SM; overall, however, the higher sparsity of the system under consideration leads to (much) lower TPR and JI scores than the ones obtained when analysing the WTW.

very fine-grained kind of information, i.e. the exact position of the connections populating the training set, while the CM takes as input a much coarser one, i.e. (just) the number of connections that are incident to each node (its degree).

While the first consideration is in agreement with the results of [7], the second is not. Such a discrepancy may

be due to several reasons: *i*) there, the considered systems are supply chains, represented as binary, directed networks, while, here, the binary, undirected representation of the world trade and of a financial system has been considered. While these are not big differences, per se, the chosen representation affects the way models are defined, as well as the number and type of ‘exogenous’

features (e.g. industry, location, size) that can be employed - the FM implemented in [7] is undirected in nature, hence particularly unsuited to model directed configurations characterised by a small value of reciprocity such as production networks; *ii*) there, local, topological information such as the one encoded into the degree sequence(s) has been apparently ignored. Here, instead, it represents the backbone of many of the models taking as inputs ‘endogenous’ features; *iii*) there, algorithms are trained on subsets of the original dataset, identified to contain both connected and unconnected pairs of nodes - more specifically, \mathcal{U} is split into training and test set, i.e. $\mathcal{U} = \mathcal{U}^{tr} \cup \mathcal{U}^{te}$, and, then, \mathcal{U}^{tr} is sampled, the collected information consisting of one observation for each pair of firms that has been drawn, i.e. whether the two firms are connected or not, plus a vector of features. Here, instead, all algorithms are trained on the same (incomplete) portion of the dataset of interest, to let all of them start on equal footing. Still, we have carried out an additional set of comparisons, more in line with the approach pursued in [7]; the results are shown in Appendix C: as evident upon inspecting the figures there, very similar considerations to the ones above hold true.

Overall, machine learning algorithms need to be fed with (much) more information than that required by white-box ones - what is required to make predictions on the ‘test’ portion of the dataset is, in fact, the exact knowledge of the ‘training’ portion of the dataset - in order to achieve a performance that is not necessarily better. While such a need may even represent an advantage when considering a specific dataset, it turns out to constitute a limitation when coming to generalise, as machine learning approaches either perform quite poorly (e.g. whenever trained on a dataset to predict the missing links of another) or cannot perform at all (e.g. whenever in presence of missing information). White-box models, on the contrary, perform robustly: examples are provided by the network reconstruction tasks carried out in [9, 45], where the considered systems have been fully reconstructed by (solely) employing the strengths of nodes and (an estimation of) the link density.

Still, our motivation, here, is not that of challenging the performance of machine learning approaches, rather checking under which conditions they can be said to outperform white-box models in link prediction tasks: what emerges from our analysis is that answering such a question crucially depends on the way these exercises are carried out.

VI. ACKNOWLEDGMENTS

This work has been supported by the following projects: ‘RE-Net - Reconstructing economic networks: from physics to machine learning and back’ - 2022MTBB22, Funded by the European Union Next

Generation EU, PNRR Mission 4 Component 2 Investment 1.1, CUP: D53D23002330006; ‘C2T - From Crises to Theory: towards a science of resilience and recovery for economic and financial systems’ - P2022E93B8, Funded by the European Union Next Generation EU, PNRR Mission 4 Component 2 Investment 1.1, CUP: D53D23019330001; ‘SoBigData RI PPP - SoBigData RI Preparatory Phase Project’, funded by the European Union under the scheme HORIZON-INFRA-2021-DEV-02-01, preparatory phase of new ESFRI research infrastructure projects, G.A. 101079043; ‘FAIR - Future Artificial Intelligence Research’ - Spoke 1 ‘Human-centered AI’, funded by the European Commission under the Next Generation EU program, PNRR Mission 4 Component 2 Investment 3.1, G.A. PE00000013.

The authors thank Mattia Marzi for insightful discussions.

VII. AUTHOR CONTRIBUTIONS

Study conception and design: FS, GC, TS. Data collection: FS. Analysis and interpretation of results: FS, GC, TS. Draft manuscript preparation: FS, GC, TS. Draft manuscript revision: FS, GC, TS.

VIII. COMPETING INTERESTS

The authors declare no competing interests.

* francesca.santucci@imtlucca.it

- [1] T. Squartini, G. Caldarelli, G. Cimini, A. Gabrielli, and D. Garlaschelli, [Physics Reports Reconstruction methods for networks: The case of economic and financial systems](#), **757**, 1 (2018).
- [2] L. Lü and T. Zhou, [Physica A: Statistical Mechanics and its Applications](#) **390**, 1150 (2011).
- [3] D. Liben-Nowell and J. Kleinberg, [Journal of the American Society for Information Science and Technology](#) **58**, 1019 (2007), eprint: <https://onlinelibrary.wiley.com/doi/pdf/10.1002/asi.20591>.
- [4] G. Berlusconi, F. Calderoni, N. Parolini, M. Verani, and C. Piccardi, [PLOS ONE](#) **11**, e0154244 (2016), publisher: Public Library of Science.
- [5] M. Jalili, Y. Orouskhani, M. Asgari, N. Alipourfard, and M. Perc, [Royal Society Open Science](#) **4**, 160863 (2017), publisher: Royal Society.
- [6] F. Parisi, G. Caldarelli, and T. Squartini, [Applied Network Science](#) **3**, 10.1007/s41109-018-0073-4 (2018), publisher: Springer Science and Business Media Deutschland GmbH.
- [7] L. Mungo, F. Lafond, P. Astudillo-Estevez, and J. D. Farmer, [Journal of Economic Dynamics and Control](#) **148**, 104607 (2023).

[8] M. Bardoscia, P. Barucca, S. Battiston, F. Caccioli, G. Cimini, D. Garlaschelli, F. Saracco, T. Squartini, and G. Caldarelli, *Nature Reviews Physics* **3**, 490 (2021), publisher: Nature Publishing Group.

[9] L. N. Ialongo, C. de Valk, E. Marchese, F. Jansen, H. Zmarrou, T. Squartini, and D. Garlaschelli, *Scientific Reports* **12**, 11847 (2022), publisher: Nature Publishing Group.

[10] A. L. Barabási and R. Albert, *Science* **286**, 509 (1999).

[11] T. Zhou, L. Lü, and Y.-C. Zhang, *The European Physical Journal B* **71**, 623 (2009).

[12] L. Katz, *Psychometrika* **18**, 39 (1953).

[13] S. Brin and L. Page, *Computer Networks and ISDN Systems Proceedings of the Seventh International World Wide Web Conference*, **30**, 107 (1998).

[14] P. Y. Chebotarev and E. Shamis, *The Matrix-Forest Theorem and Measuring Relations in Small Social Groups* (1997).

[15] G. Jeh and J. Widom, *SimRank: A Measure of Structural-Context Similarity* (2002).

[16] W. Liu and L. Lü, *Europhysics Letters* **89**, 58007 (2010).

[17] A. Clauset, C. Moore, and M. E. J. Newman, *Nature* **453**, 98 (2008), publisher: Nature Publishing Group.

[18] R. Guimerà and M. Sales-Pardo, *Proceedings of the National Academy of Sciences of the United States of America* **106**, 22073 (2009).

[19] F. Adriaens, A. Mara, J. Lijffijt, and T. De Bie, in *Proceedings - 2020 IEEE 7th International Conference on Data Science and Advanced Analytics, DSAA 2020* (Institute of Electrical and Electronics Engineers Inc., 2020) pp. 70–80.

[20] N. Friedman, L. Getoor, D. Koller, and A. Pfeffer, in *IJCAI International Joint Conference on Artificial Intelligence*, Vol. 2 (International Joint Conferences on Artificial Intelligence, 1999) pp. 1300–1307, iSSN: 1045-0823.

[21] K. Yu, W. Chu, S. Yu, V. Tresp, and Z. Xu, in *Advances in Neural Information Processing Systems*, Vol. 19 (MIT Press, 2006).

[22] W. Isard, *The Quarterly Journal of Economics* **68**, 305 (1954).

[23] J. Tinbergen, *Shaping the World Economy; Suggestions for an International Economic Policy* (1962).

[24] F. Pedregosa, G. Varoquaux, A. Gramfort, V. Michel, B. Thirion, O. Grisel, M. Blondel, P. Prettenhofer, R. Weiss, V. Dubourg, J. Vanderplas, A. Passos, D. Cournapeau, M. Brucher, M. Perrot, and \. Duchesnay, *Journal of Machine Learning Research* **12**, 2825 (2011).

[25] J. H. Friedman, *Greedy function approximation: a gradient boosting machine*, Tech. Rep. 5 (The Annals of Statistics, 2001) publication Title: The Annals of Statistics Volume: 29.

[26] G. Ke, Q. Meng, T. Finley, T. Wang, W. Chen, W. Ma, Q. Ye, and T.-Y. Liu, in *Advances in neural information processing systems*, Vol. 30, edited by I. Guyon, U. V. Luxburg, S. Bengio, H. Wallach, R. Fergus, S. Vishwanathan, and R. Garnett (Curran Associates, Inc., 2017).

[27] J. Park and M. E. J. Newman, *Physical Review E* **70**, 066117 (2004), publisher: American Physical Society.

[28] G. Bianconi, *Europhysics Letters* **81**, 28005 (2007).

[29] T. Squartini and D. Garlaschelli, *New Journal of Physics* **13**, 10.1088/1367-2630/13/8/083001 (2011).

[30] A. Fronczak, *Physical Review E* **85**, 10.1103/PhysRevE.85.056113 (2012).

[31] T. Squartini, R. Mastrandrea, and D. Garlaschelli, *New Journal of Physics* **17**, 023052 (2015), publisher: IOP Publishing.

[32] F. Saracco, R. Di Clemente, A. Gabrielli, and T. Squartini, *Scientific Reports* **5**, 10595 (2015), publisher: Nature Publishing Group.

[33] G. Cimini, T. Squartini, F. Saracco, D. Garlaschelli, A. Gabrielli, and G. Caldarelli, *Nature Reviews Physics* **1**, 58 (2019), publisher: Nature Publishing Group.

[34] S. N. Dorogovtsev, J. F. F. Mendes, and A. N. Samukhin, *Nucl. Phys. B* **666**, 396 (2003), eprint: cond-mat/0204111.

[35] J. Park and M. E. J. Newman, *Physical Review E* **68**, 026112 (2003), publisher: American Physical Society.

[36] D. Garlaschelli and M. I. Loffredo, *Physical Review E* **78**, 015101 (2008), publisher: American Physical Society.

[37] N. Vallarano, M. Bruno, E. Marchese, G. Trapani, F. Saracco, G. Cimini, M. Zanon, and T. Squartini, *Scientific Reports* **11**, 10.1038/s41598-021-93830-4 (2021).

[38] M. Di Vece, *Physical Review E* **108**, 10.1103/PhysRevE.108.054301 (2023).

[39] M. Marzi, F. Giuffrida, D. Garlaschelli, and T. Squartini, *Reproducing the first and second moment of empirical degree distributions* (2025), arXiv:2505.10373 [physics].

[40] G. Cimini, R. Mastrandrea, and T. Squartini, *Reconstructing Networks* (Cambridge University Press, 2021) google-Books-ID: 3U0_EAAAQBAJ.

[41] F. Picciolo, T. Squartini, F. Ruzzentini, R. Basosi, and D. Garlaschelli, in *2012 Eighth International Conference on Signal Image Technology and Internet Based Systems* (2012) pp. 784–792.

[42] G. Bianconi, *Information theory of spatial network ensembles* (2022), arXiv:2206.05614 [cond-mat].

[43] G. Caldarelli, A. Capocci, P. De Los Rios, and M. A. Muñoz, *Physical Review Letters* **89**, 10.1103/PhysRevLett.89.258702 (2002).

[44] D. Garlaschelli and M. I. Loffredo, *Physical Review Letters* **93**, 10.1103/PhysRevLett.93.188701 (2004), publisher: American Physical Society.

[45] G. Cimini, T. Squartini, D. Garlaschelli, and A. Gabrielli, *Scientific Reports* **5**, 15758 (2015), publisher: Nature Publishing Group.

[46] J. Park and M. E. J. Newman, *Physical Review E* **70**, 066146 (2004), publisher: American Physical Society.

[47] M. Bolfe, F. L. Metz, E. Guzmán-González, and I. P. Castillo, *Physical Review E* **104**, 014147 (2021), arXiv:2102.09629 [cond-mat].

[48] K. S. Gleditsch, *Journal of Conflict Resolution* **46**, 712 (2002), publisher: Peace Science Society (International).

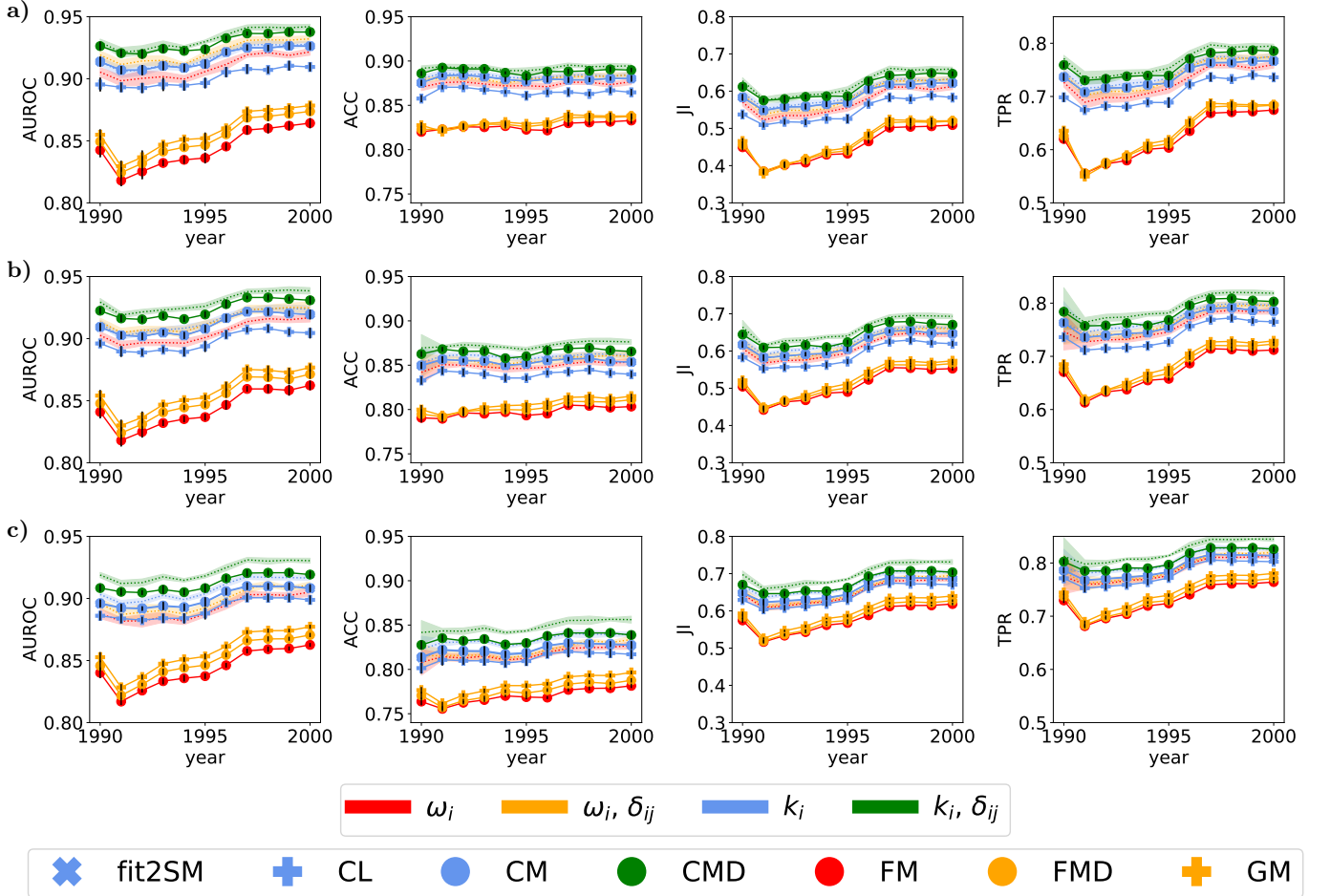


Figure A1: Performance of the models, measured in terms of AUROC (first column), ACC (second column), JI (third column) and TPR (fourth column), for all years of the WTW and for three, different shares of removed links, i.e. 20% (row a), 30% (row b), 50% (row c). The dashed lines and shaded areas correspond to the average values and standard deviations of the performances of the GBDT while coloured symbols and vertical, black bars indicate the average values and standard deviations of the performances of white-box models, with different colours corresponding to different features (see the legend).

APPENDIX A. MISSING LINKS PREDICTION ON THE WORLD TRADE WEB

Figure A1 depicts the performance of our models for different shares of removed links: as it can be appreciated, the performance of the CMD remains high up to a large percentage of missing links; still, the performance of the GBDT deteriorates to a lesser extent than the one of white-box models.

quarter	N	L	c	\bar{k}
2000 - Q01	181	5483	0.337	60.59
2000 - Q03	178	5205	0.330	58.48
2010 - Q01	113	1433	0.226	25.36
2010 - Q03	107	1476	0.260	27.59
month	N	L	c	\bar{k}
2000 - M01	177	3634	0.230	41.06
2000 - M08	175	3403	0.224	38.89
2010 - M01	102	1014	0.197	19.88
2010 - M08	97	920	0.198	18.97
week	N	L	c	\bar{k}
2000 - W01	170	1428	0.099	16.80
2000 - W30	167	1493	0.108	17.88
2010 - W01	82	346	0.104	8.44
2010 - W30	90	423	0.106	9.40
day	N	L	c	\bar{k}
2000 - 01 - 03	149	523	0.047	7.02
2005 - 04 - 15	108	320	0.055	5.93
2010 - 08 - 30	72	166	0.065	4.61

Table IV: Basic statistics concerning the eMID dataset [39], aggregated at the quarterly, monthly, weekly and daily level. The table shows the total number of banks N , the total number of links L , the network density c and the average degree \bar{k} for each aggregation scale.

APPENDIX B.

MISSING LINKS PREDICTION ON THE ELECTRONIC MARKET FOR INTERBANK DEPOSITS

Table IV reports the basic statistics for each aggregation scale. Figure B1 depicts the performance of our models for different aggregation scales: as it can be appreciated, very similar results to the ones characterising the yearly aggregation level are obtained.

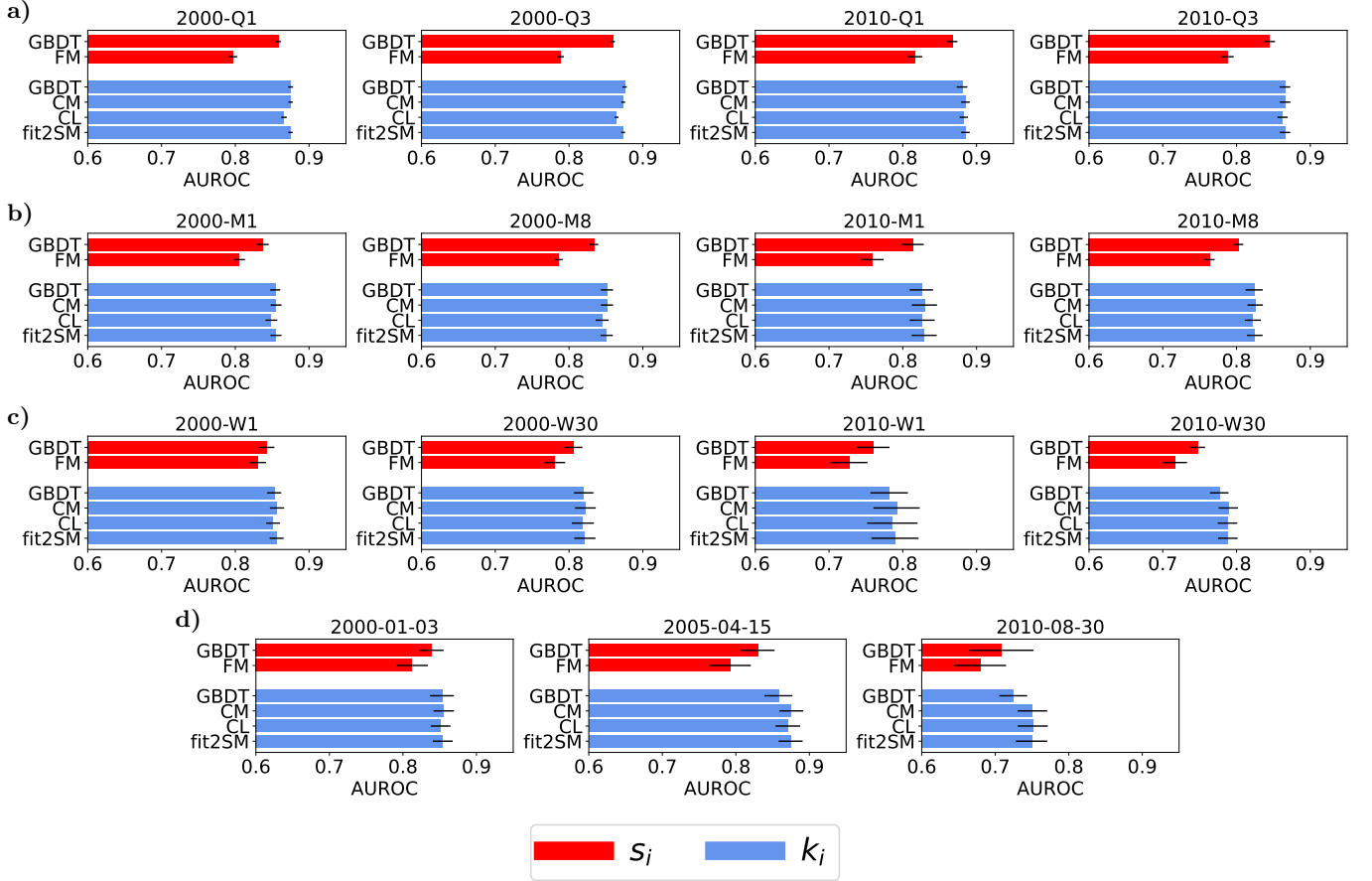


Figure B1: Performance of the models, measured in terms of AUROC, for snapshots of eMID at different aggregation levels: quarterly (row a), monthly (row b), weekly (row c) and daily (row d). The upper bar in each panel, marked with a diagonal pattern, corresponds to the black-box GBDT. We have randomly selected the 20% of links 10 times to populate \mathcal{E}^{miss} and generate $\mathcal{E}^{obs} = \mathcal{E} \setminus \mathcal{E}^{miss}$; each statistical indicator has, then, been averaged over such samples, the standard deviation being represented by a horizontal, black bar. The FM has been implemented by replacing ω_i with s_i in eq. 33 (see the colour legend). As for the WTW, each ‘endogenous’ instance of the GBDT performs in a way that is comparable to that of its purely structural, white-box counterpart; the results are overall consistent across aggregation levels.

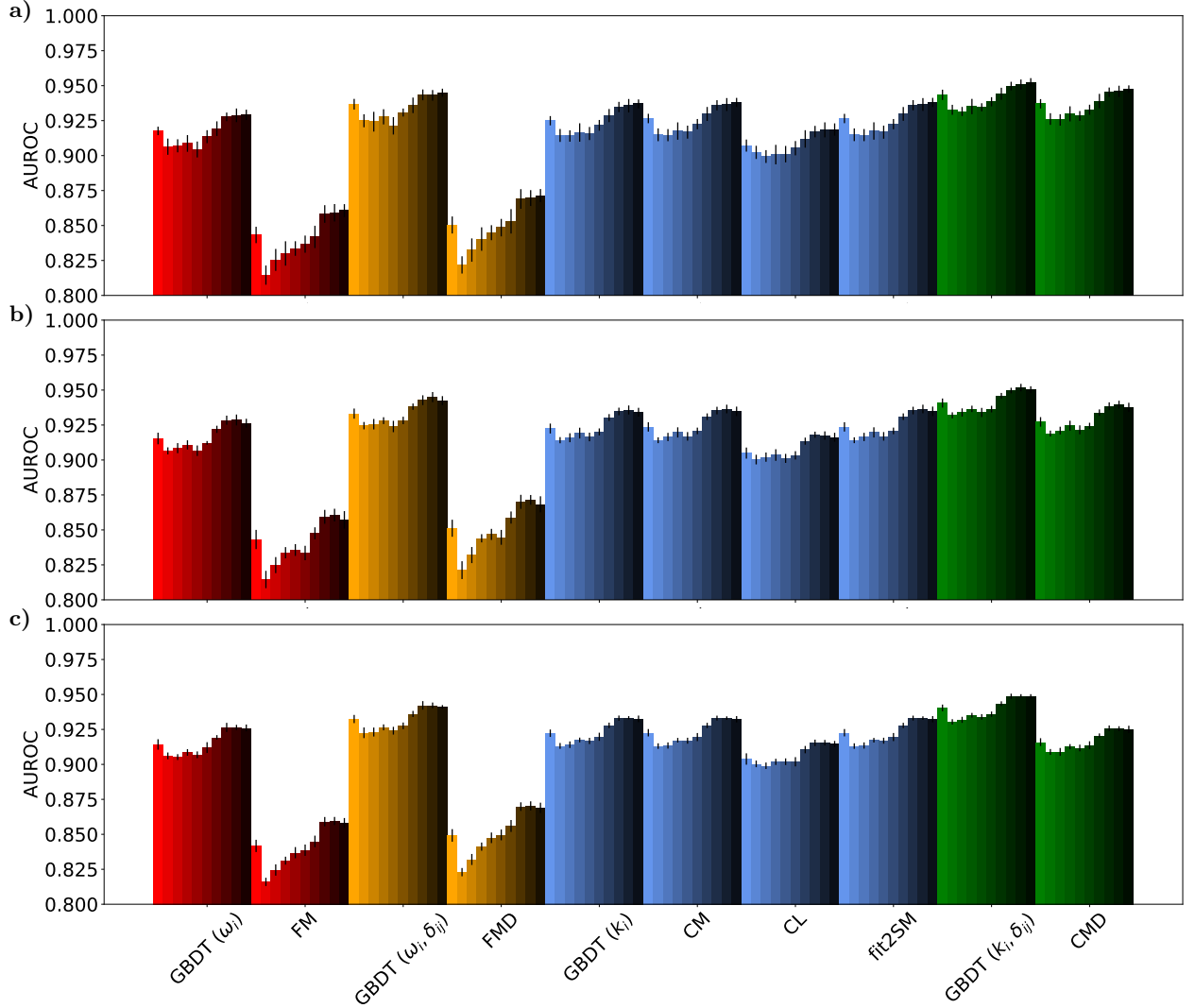


Figure C1: Performance of the models, measured in terms of AUROC, for all years of the World Trade Web (darker shades correspond to more recent years). We have randomly selected the 10% (row **a**), the 20% (row **b**) and the 30% (row **c**) of node pairs 10 times to populate the test set, on which the prediction is performed after having trained the model on the remaining pairs of nodes. Each statistical indicator has, then, been averaged over such samples, the standard deviation being represented by a vertical, black bar. The results are in agreement with those reported in the main text, as each ‘endogenous’ instance of the GBDT performs in a way that is comparable to that of its purely structural, white-box counterparts - especially for what concerns the CM and the fit2SM.

APPENDIX C. MISSING LINKS PREDICTION IN A DIFFERENT SETTING

Another, common setting for prediction - similar to the one adopted in [7] - consists in randomly splitting all node pairs into a training and a test set, i.e. $\mathcal{U} = \mathcal{U}^{tr} \cup \mathcal{U}^{te}$: the training set is, then, identified with $\mathbf{D}^{tr} = \{\mathbf{x}_{ij}, a_{ij}\}_{ij \in \mathcal{U}^{tr}}$ and the prediction is performed on $\mathbf{D}^{te} = \{a_{ij}\}_{ij \in \mathcal{U}^{te}}$. As the evaluation of ‘endogenous’ features is based on the links populating \mathcal{U}^{tr} , this is equivalent to treating all pairs of nodes in \mathcal{U}^{te} as unconnected.

The results, shown in figure C1, are in agreement with those reported in the main text, as each ‘endogenous’ instance of the GBDT performs in a way that is comparable to that of its purely structural, white-box counterparts - especially for what concerns the CM and the fit2SM. To be noticed that the performance of the GBDT taking as inputs both ‘exogenous’ and ‘endogenous’ features deteriorates to a lesser extent than the one of the CMD, i.e. its white-box counterpart, as the size of the training set decreases.